A perfusable vascularized full-thickness skin model for potential topical and systemic applications

Sacha Salameh, Nicolas Tissot, Kevin Cache, Joaquim Lima, Itaru Suzuki, Paulo André Marinho, Maité Rielland, Jérémie Soeur, Shoji Takeuchi, Stéphane Germain, et al.

Biofabrication

International Society for Biofabrication

PAPER • OPEN ACCESS

A perfusable vascularized full-thickness skin model for potential topical and systemic applications

Biofabrication

PAPER

A perfusable vascularized full-thickness skin model for potential topical and systemic applications

Sacha Salameh[1,2,*], Nicolas Tissot[1], Kevin Cache[1], Joaquim Lima[1], Itaru Suzuki[1], Paulo André Marinho[1], Maité Rielland[1], Jérémie Soeur[1], Shoji Takeuchi[4], Stéphane Germain[3,5] and Lionel Breton[1,5]

[1] L'Oréal Research and Innovation, Aulnay-sous-Bois, France
[2] Sorbonne Université, Collège Doctoral, F-75005 Paris, France
[3] Center for Interdisciplinary Research in Biology (CIRB), College de France, CNRS, INSERM, PSL Research University, Paris, France
[4] Department of Mechano-Informatics, Graduate School of Information Science and Technology, The University of Tokyo, 7-3-1 Hongo, Bunkyo-ku, Tokyo 113-8656, Japan
[5] Equal contribution.
[*] Author to whom any correspondence should be addressed.

E-mail: sacha.salameh@rd.loreal.com

Keywords: reconstructed skin, tissue engineering, vascularization, vasculogenesis, angiogenesis, perfusion

Supplementary material for this article is available online

OPEN ACCESS

RECEIVED
16 December 2020

REVISED
20 April 2021

ACCEPTED FOR PUBLICATION
28 April 2021

PUBLISHED
14 May 2021

Abstract

Vascularization of reconstructed tissues is one of the remaining hurdles to be considered to improve both the functionality and viability of skin grafts and the relevance of *in vitro* applications. Our study, therefore, sought to develop a perfusable vascularized full-thickness skin equivalent that comprises a more complex blood vasculature compared to existing models. We combined molding, auto-assembly and microfluidics techniques in order to create a vascularized skin equivalent representing (a) a differentiated epidermis with a physiological organization and correctly expressing K14, K10, Involucrin, TGM1 and Filaggrin, (b) three perfusable vascular channels with angiogenic sprouts stained with VE-Caderin and Collagen IV, (c) an adjacent microvascular network created via vasculogenesis and connected to the sprouting macrovessels. Histological analysis and immunostaining of CD31, Collagen IV, Perlecan and Laminin proved the integrity of vascular constructs. In order to validate the vascularized skin potential of topical and systemic applications, caffeine and minoxidil, two compounds with different chemical properties, were topically applied to measure skin permeability and benzo[a]pyrene pollutant was systemically applied to evaluate systemic delivery. Our results demonstrated that perfusion of skin reconstructs and the presence of a complex vascular plexus resulted in a more predictive and reliable model to assess respectively topical and systemic applications. This model is therefore aimed at furthering drug discovery and improving clinical translation in dermatology.

1. Introduction

Tissue engineering and regenerative medicine hold high promises for organ replacement and development of novel therapies. Being the largest human organ, the loss of skin integrity due to injury or illness results in a substantial physiologic imbalance and ultimately in severe disability or death. The skin was the first reconstructed tissue generated by tissue engineering approach [1] for the treatment of burns, surgical scars, and plastic surgery [2]. Skin models are also used in the evaluation of active compounds and drugs' efficacy and toxicity in cosmetic and pharmaceutical research, especially after the ban of animal testing in cosmetic research in 2013 (European Community directive 93/35/EEC) [3–5].

In the '70s Rheinwald and Green [6] managed to culture epidermal human keratinocytes. Since then, many skin substitutes have been developed to reproduce physiological functions and get closer to *in vivo* skin. For instance, endothelial cells [7], immune cells [8], and melanocytes [9] have been included in 3D skin equivalents. Recently, more

advanced and complex skin substitutes were published by the integration of hair follicles [10], mature adipocytes in a three-layered skin equivalent [11], sebocytes organoids derived from human induced pluripotent stem cells (hIPS) [12], IPS derived sensory neurons, and Schwann cells with endothelial cells in an innervated engineered skin sponge model [13], etc. Moreover, recent interest has focused on transferring various micro-physiological organ models, including skin, onto microfluidic platforms [14–18]. These skin-on-a-chip models enable physiologically relevant transport of nutrients and exogenous substances to the skin tissue, better control over physical and chemical factors in the cell microenvironment [19], and more reliable evaluation of drug candidates in terms of toxicity, efficacy, and delivery compared to static conditions [20].

Nevertheless, reconstructing thick or complex tissues that faithfully recapitulate all the functions of the *in vivo* skin is still a challenge [21]. One of the main limitations is the lack of vascularization and perfusion in reconstructed tissues.

Given that the diffusion coefficient of oxygen is limited to 200 μm in human tissues [22, 23], >200 μm thick skin constructs might encounter necrosis because of hypoxia [24, 25]. Therefore, developing perfusable vascular networks in order to blunt hypoxia and improve viability is mandatory. For instance, prevascularization in skin graft for clinical application accelerates anastomosis *in vivo* with the host vascular network and thereby improves oxygen and nutrient supply [26]. *in vitro*, generating a skin-equivalent with hair follicles as dense as what we find *in vivo* could result in a necrotic core if the tissue is not prevascularized [10]. Additionally, vascularized skin reconstructs represent invaluable tools for basic research (e.g. study vascular remodeling during wound healing, aging, cancer, etc) but also for topical and systemic evaluation (e.g. screening pro- and anti-angiogenic drugs, evaluation of systemic toxicity, percutaneous absorption of chemicals and drugs) [27–30]. Certainly, having a perfusable vascular network in skin equivalents makes more relevant the evaluation of systemic delivery of substances, but also the study of systemic exposure or inflammation responses which could not be properly assessed with existing skin models. Improving vascularization of tissue-engineered constructs has therefore gained interest in the last decade [31]. Many strategies have been developed to improve or accelerate vascular growth in engineered tissues either *in vivo* relying on improving the angiogenesis process from the host tissue into the implant [32–35] or by prevascularization of the engineered tissue. Different *in vitro* techniques were thus developed including sparse cells seeding into scaffolds or hydrogels [36–38], cell sheet strategy [39–41], reuse of biological vascular structures [42–45], bioprinting [46–48], and vascular network patterning [49–52] to be able to perfuse the construct.

However, the generation of a vascularized reconstructed full-thickness skin that gathers a properly differentiated epidermis as well as *in vivo*-like perfused vasculature still represents a major challenge. Several studies reported vascularized skin substitutes that cannot be perfused [30, 40, 41, 53–55] which is a limitation for systemic applications. Some others developed perfusable vessel-like constructs in cell-free hydrogels that better mimic blood flow in vascular networks, however do not allow the study of the vascularization role or systemic exposure effect on surrounding tissues [47, 50–52, 55, 56]. On the other hand, vascular networks were also generated in a perfusable dermis substitute but these constructs still lacked an epidermal layer which is a limitation for topical applications [57]. Nonetheless, the few existing models of perfusable vascularized full-thickness skin are limited. Today, and to our knowledge, there are only four developed *in vitro* models of perfusable vascularized reconstructed full-thickness skin. Groeber *et al* [43] used a porcine jejunum as a scaffold but this model cannot be used in large-scale production as it relies on the use of an animal organ. Abaci *et al* [58] used bioprinting to engineer a spatially controlled vascular pattern in a 3D skin reconstruct but their skin lacks microvascularization and epidermal differentiation layers. Mori *et al* [28] developed a device with anchoring structures and connectors allowing the reconstruction of a perfusable reconstructed skin. However, this model displayed one macrochannel seeded with endothelial cells without a microvascular network in the dermis and with thin layers of keratinocytes that did not recapitulate full epidermis differentiation. Using the same device with stretchable material, the authors cultured this skin-equivalent under stretching and perfusion conditions. They showed that perfusion and stretch stimuli improved skin-equivalent morphology [59]. Kim *et al* [60] used 3D printing to engineer perfusable vascularized skin with a hypodermis, dermis, and epidermis. However, the vasculature of the skin equivalent remained a unique macrochannel lacking the physiological cutaneous microvascularization.

In this study, by combining molding and auto-assembly techniques as well as microfluidics, we developed for the first time a fully vascularized perfusable reconstructed skin that comprises a differentiated epidermis containing all the layers of the *in vivo* structure, perfusable macrovessels with angiogenic sprouts, and a microvascular network with capillaries organized by vasculogenesis in the dermis part. We further showed that this model is relevant for studying both systemic drug delivery and skin permeability.

2. Materials and methods

2.1. Cell culture reagents

DMEM high glucose GlutaMAX, Ham's F-12 Nutrient Mix GlutaMAX, MEM supplemented with non-essential amino acid, L-glutamine, sodium pyruvate, phosphate-buffered saline without Mg^{2+} and Ca^{2+} (PBS-), Trypsin-EDTA, antibiotic–antimycotic solution (100 U ml^{-1} penicillin-streptomycin; 0.25 μg ml^{-1} amphotericin B) were purchased from Invitrogen (Carlsbad, CA, USA). L-Ascorbic acid 2-phosphate sesquimagnesium salt hydrate (Vitamin C), human recombinant epidermal growth factor (EGF), adenine hydrochloride, hydrocortisone 21-hemisuccinate sodium, (-) isoproterenol hydrochloride, 3.3′.5-triiodo-l-thyronine sodium 95%, apo-transferrin, were purchased from Sigma (St. Louis, MO, USA). VEGFA-$_{165}$, Endothelial Cell Growth Medium 2 (ECGM2), endothelial basal medium (EBM), Supplement Pack endothelial cell GM2 were purchased from Promocell (Heidelberg, Germany). Fetal bovine serum (FBS) was purchased from PAN-Biotech GmbH (Aidenbach, Germany). Bovine type I collagen solution (ACI-100) was purchased from Symatese (Chaponost, France).

2.2. Cell culture

Normal human dermal fibroblasts (NHDFs) and normal human epidermal keratinocytes (NHEKs) were provided by Episkin (Lyon, France) and used at passage 8 and passage 2, respectively. Human umbilical vein endothelial cells (HUVECs) were purchased from PromoCell GmbH (Heidelberg, Germany) and used at passage 4. HUVECs were transduced at passage 2 using EGFP-Puro or Turbo-RFP lentiviruses (Vectalys, France) with a titer of 4.2 $\times$ 10^9 or 5.4 $\times$ 10^9 TU ml^{-1} respectively and used at passage 5 in 3D cultures. NHDFs were maintained in DMEM 10% FBS, 1% antibiotic-antimycotic solution, and HUVECs in ECGM-2 supplemented with 1% antibiotic–antimycotic solution. NHEKs were grown on irradiated primary mouse embryonic fibroblasts, using keratinocyte medium containing DMEM and Ham's F12 at a ratio of 3:1 supplemented with 180 μM adenine, 10 ng ml^{-1} epidermal growth factor, 0.4 μg ml^{-1} hydrocortisone, 5 μg ml^{-1} insulin, 2 nM triiodo-L-thyronine, 1 μM isoproterenol, 1% antibiotics–antimycotic solution, and 10% FBS. All cells were grown at 37 °C in 5% CO_2. The medium was changed three times a week.

2.3. Reconstruction of the skin equivalent

The culture device was as previously described [28]. Here, three nylon wires (0.55 mm diameter) were strung across the connectors before sterilization using 70% ethanol and UV light. Devices were then treated for 15 min using a plasma etcher (Harrick Plasma, Ithaca, NY USA). The devices were then filled with 1.5 mg ml^{-1} of a neutralized solution of bovine type I collagen and 2 $\times$ 10^6 ml^{-1} NHDFs prepared as previously described [61, 62] and incubated at 37 °C for 30/60 min until the collagen gel formed a dermis-like layer. The final number of NHDFs was 0.5 $\times$ 10^6 cells per lattice. Dermal substitutes were incubated in NHDF 3D medium (DMEM containing 10% FBS, 100 U ml^{-1} penicillin-streptomycin, 0.25 μg ml^{-1} amphotericin B, and 70 μg ml^{-1} ascorbic acid) for 5 d to allow contraction. The medium was then changed to ECGM-2. Nylon wires were removed and hollow channels were filled with 200 μl ECGM-2 containing 8 $\times$ 10^5 HUVECs using a syringe pump at a flow rate of 6.5 ml h^{-1} (KD Scientific, Holliston, MA, USA). At this time point, once nylon wires are removed, the contraction of the collagen gel is enough to maintain a tubular structure without causing damage or collapsing upon removal. The device was inverted for 30 min to coat the upper half of the channels with HUVECs and then inverted again and incubated for 24 h in ECGM-2 to allow the endothelial cells adhesion. Subsequently, 6 $\times$ 10^5 keratinocytes were seeded on the dermal layer and immersed in DMEM/F12 immersion medium (DMEM and Ham's F12 at a ratio of 3:1 supplemented with 180 μM adenine, 10 ng ml^{-1} hEGF, 0.4 μg ml^{-1} hydrocortisone, 5 μg ml^{-1} insulin, 2 nM triiodo-L-thyronine, 1 μM isoproterenol, 5 μg ml^{-1} apo-transferrin, 100 U ml^{-1} penicillin–streptomycin, 0.25 μg ml^{-1} amphotericin B, 1 nM VEGF-A_{165} and 10% FBS). The central channel was then perfused at 2–3 ml h^{-1} using a peristaltic pump (SJ-1211II-L, ATTO Corp., Tokyo, Japan). After 3 d of immersion, the skin equivalent was lifted to the air–liquid interface for 7 d to induce stratification of the epidermal layer using DMEM/F12 emersion medium (DMEM and Ham's F12 at a ratio of 3:1 supplemented with 0.4 μg ml^{-1} hydrocortisone, 5 μg ml^{-1} insulin, 1 nM VEGF, 100 U ml^{-1} de penicillin-streptomycin, 0.25 μg ml^{-1} amphotericin B and 1% FBS). The flow rate was increased to 6.5 ml h^{-1} and perfusion was maintained until the end of the culture (17 d in total). The media was changed every other day.

To induce vasculogenesis, half the volume of the neutralized collagen/fibroblasts mix was poured until it reached the nylon wires. The device was then incubated at 37 °C for 20–30 min until collagen gelation and 6 $\times$ 10^5 HUVECs transduced with Turbo-RFP lentiviruses (Vectalys, France) (RFP-HUVEC) were then seeded as a monolayer and incubated for 1 h to allow cell adhesion. After 20–30 min of incubation, an equal volume of collagen/fibroblasts was poured to cover the RFP-HUVEC layer. The dermal layer was incubated in NHFD 3D/ECGM2 mix medium (44% DMEM glutamax and 47% Endothelial Basal Medium EBM supplemented with Supplement Pack endothelial cell GM2, 6.3% FBS, 1% antibiotic–antimycotic, 70 μg ml^{-1} ascorbic acid) for 5 d. Then the same protocol as described above was

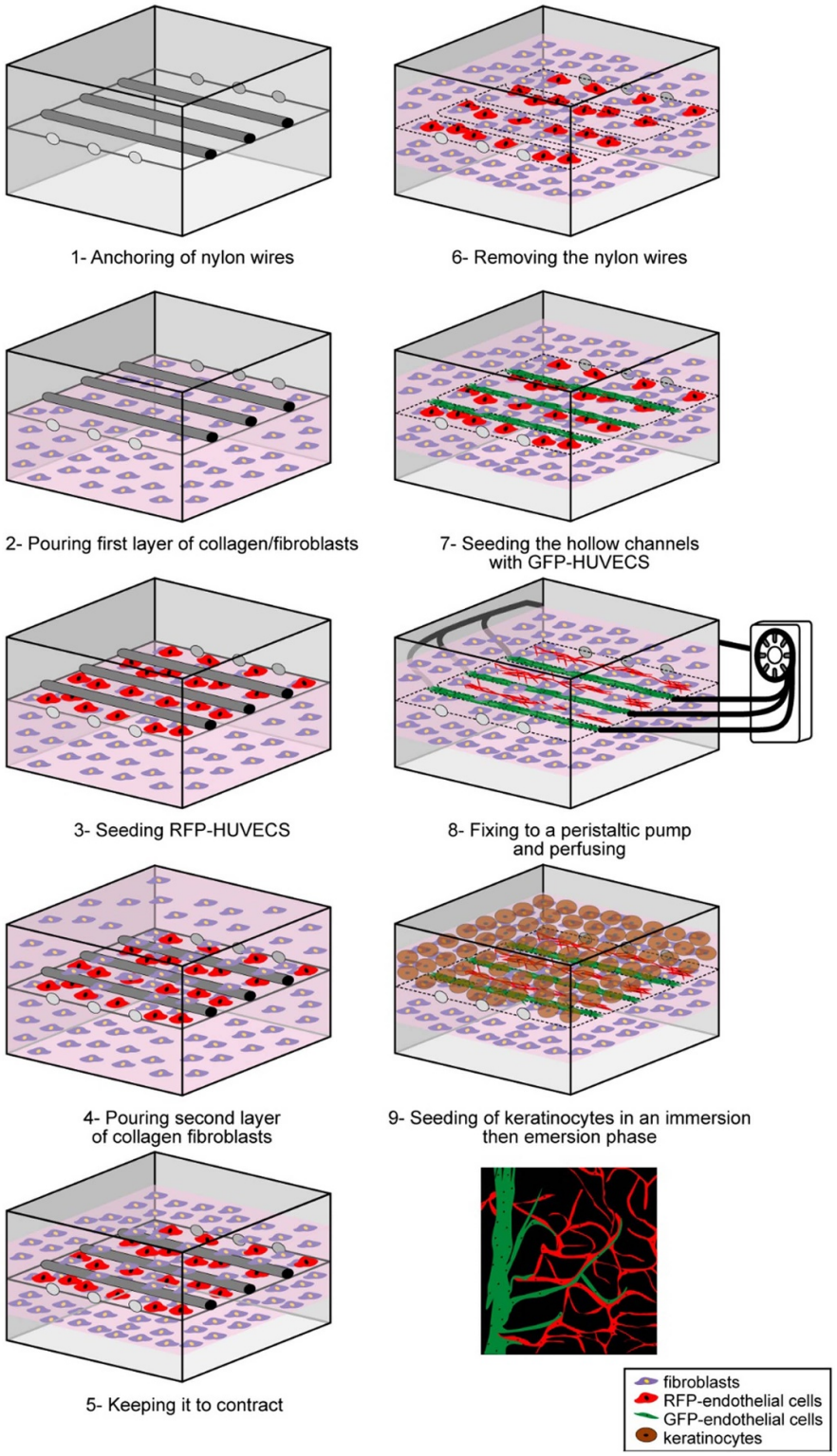

Figure 1. Schematic illustration showing the development of the perfusable vascularized reconstructed skin model.

followed, except that hollow channels were seeded with HUVECs transduced with EGFP lentiviruses (EGFP-HUVEC) (figure 1).

2.4. Histological analyses

Morphologies of the skin equivalent and vascular channels were analyzed using hematoxylin, eosin, and saffron (HES) staining or immunostaining.

Immunofluorescent stainings were performed on 7 μm frozen sections fixed in cold acetone, blocked in bovine albumin serum (BSA)-10% normal goat serum (SP-004-vx10, Diagomics, France) and incubated 1 h at room temperature (RT) or O/N at 4 °C with diluted primary antibodies in 1% BSA: Laminin alpha 5 (1:20 Dako M0638,Agilent, USA), Collagen IV (COLL IV) (1:50 Dako M0785, Agilent, USA),

Perlecan (1:100 ab26265, Abcam, United kingdom), CD31 (1:20 Dako M0823, Agilent, USA), Alpha Actin (1:100 sc32251, Santa Cruz,USA), Keratin 14 (K14) (1:20 Progen 10003, Progen, USA), Keratin 10 (K10) (1:100 Dako M7002, Agilent, USA), Involucrin (INV) (1:50 BTI J64013-AB,Biotechnology Ltd, UK), transglutaminase 1 (TGM1) (1:500 NBP2-34062, Novus Biologicals, USA), filaggrin (FIL) (1:200 sc66192, Santa-Cruz, USA). Sections were washed with PBS- and incubated with secondary antibody solution (A21422 or A21428, Thermo Fisher Scientific, USA) diluted 1:500 in 1% BSA for 1 h at RT. Sections were then mounted using Prolong with DAPI (P36931, Life Technologies, USA) and observed with Nanozoomer S60 (Hamamatsu, Japan) or Nikon Microscopy Eclipse 80i (Nikon, Japan).

For whole-mount staining, samples were fixed in 4% formaldehyde (VWRC9713, VWR, USA) for 20 min. The samples were then washed with PBS- and vascular channels were filled with PBS-1% BSA using a syringe pump. After 1 h of saturation, vascular channels were filled with Collagen IV primary antibody diluted 1:50 in PBS-1% BSA (Dako M0785, Agilent, USA) and incubated for 2 h at RT. The primary antibody solution was washed out with PBS- three times for 10 min. The vascular channels were filled with secondary antibodies targeting mouse IgG coupled to Alexa Fluor 488 (A11029, Thermo Fisher Scientific, USA) diluted 1:100 in PBS-1% BSA and incubated for 1 h at RT. For VE-Cadherin, primary antibody already coupled to Alexa Fluor 488 secondary antibody (1:100 53-1449, Thermo Fisher Scientific, USA) was incubated 2 h at RT in the channels. Channels were then observed using two-photon microscopy (Leica SP8 coupled to a Spectra Physics Insight femtosecond laser, Leica Microsystems, Germany). Fluorescence signal emitted by the Alexa Fluor 488 or EGFP and by the Turbo-RFP were detected with an objective HCX APO L 10x/0.30 W (Leica Microsystems, Germany) then separated using a 560 nm dichroic mirror and detected by two non-descanned detectors (emission filter 525/50 and 585/40 for A488/EGFP and Turbo-RFP, respectively).

2.5. Measurement of skin permeability

To estimate skin barrier function, we measured skin permeation of a mix of two chemicals with different physicochemical parameters: Caffeine and Minoxidil (purity 100%) obtained from L'Oréal (Aulnay-sous-Bois, France).

The study was performed on six different skin equivalents: control samples with no channels (Lat), Channels with endothelial cells but without perfusion (ECnoP), perfused channels with endothelial cells (ECP), perfused channels without endothelial cells (noECP), Channels with endothelial cells and secondary microvascularization without perfusion (SandnoP), perfused channels with endothelial cells and secondary microvascularization (SandP). Three different batches of experiments were tested except for samples with secondary vascular plexus (SandnoP and SandP) where only one batch of three devices was evaluated.

Around 25 mg of each chemical were dissolved in 10 ml of PBS containing 0.25% (w/w) Tween 80 (723M-156-84, Fisher scientific, USA). This surfactant was added to guarantee chemical solubility in the buffer. Before application, the solution was filtered through Millex HV 0.45 μm and then quantified to determine Caffeine and Minoxidil concentrations.

To control the volume deposited on the skin equivalent, an 8 mm PTFE ring was designed. The ring was sealed on the epidermis using DERMABOND ADVANCED® (AHVM12, Ethicon, USA) to avoid leakage. Devices were placed in a static condition on a magnetic stirrer for homogenizing to respect sink conditions. An infinite dose of 300 μl cm^{-2} of the buffered solution was topically applied on the skin in the inserted ring. Each hour for the next 6 h, 300 μl were sampled from the receptor fluid under the skin equivalent. The same amount of fresh media was added in order to maintain a constant volume in each device. Samples were then diluted (1/10) in a fresh culture medium and quantified with standards curves prepared in the same culture medium (DMEM/F12 emersion medium).

The same study was performed on 8 split-thickness pig ear skin set up on a Franz cell having 2 cm^2 square areas and 3 ml receptor compartment volume. Mean thickness was measured at 1056 $\pm$ 62 μm. The receptor compartment was filled with PBS +0.25% (w/w) to guarantee sink conditions and homogenized using a magnetic stirrer. After 1 h equilibration time, skin integrity was controlled with Trans Epidermal Water Loss measurement (Vapometer, Delfin Technologies, UK). Acceptance criteria was defined (i.e. <15 g m^{-2} h^{-1}); this value was based on internal historical data [63]. An infinite dose of the buffer solution (i.e. 300 μl cm^{-2}) containing Caffeine and Minoxidil was applied to the skin. Samples were then quantified using standards curves prepared in PBS buffer.

All samples were analyzed with an LC/MS-MS system (Shimadzu Nexera LC system coupled with a mass spectrometer API 3500 (Sciex, Concord, Canada). The analytical system was managed by the software Analyst version 1.6.3. Ascentis C18 analytic columns were from Sigma-Aldrich (Saint Louis, USA) (50 $\times$ 2.1 mm, 2.7 μm) and analyses were carried out with a gradient elution using mobile phases of 0.1% formic acid (FA) in water (A) and MeOH (B). The column temperature was fixed at 50 °C, the volume of the injection was 5 μl and the flow rate was 0.8 ml min^{-1}. The ionization mode used was electrospray ionization in positive ion mode. Multiple Reaction Monitoring (MRM) was used for detection

with the following transition: Caffeine 195.0 (m/z) → 138.1(m/z) and Minoxidil 210.0 (m/z) → 164.0 (m/z). The lower limit of quantification (LLOQ) and upper limit of quantification (ULOQ) were at 0.60 and 2130 ng ml^{-1}, respectively for Caffeine and 0.51 and 1990 ng ml^{-1} respectively for Minoxidil. The cumulative amount of Caffeine and Minoxidil through the skin was plotted as a function of time. According to Fick's first law of diffusion, the slope of the linear part of the curve defined the flux at a steady state. The permeability coefficient (Kp) was obtained by the ratio of flux and the concentration (C) of the tested compound in the solution applied on the skin: $\mathrm{Kp}\ \left(\mathrm{cm\,h^{-1}}\right) = \frac{\mathrm{Flux}\left(\mu\mathrm{g\,cm^{-2}\,h^{-1}}\right)}{C\left(\mu\mathrm{g\,cm^{-3}}\right)}$ [64].

The statistic model used took into account the batch effect as a random variable and skin models as a fixed effect. This allowed the evaluation of different sources of variability i.e. inter- and intra-batch and intra-model). Considering the low number of replicates (8 for pig ear skin, 3–12 for different reconstructed skin models), a non-parametric method was used as a statistical model as variability of the data did not follow a normal distribution. The relevance of the comparison was evaluated according to the size of the effect (i.e. very small, small, moderate, strong, or very strong). Resulting P-value was adjusted using the Bonferroni method, where a statistical significance was reached if $P < 0.05$.

2.6. Systemic exposure of benzo[a]pyrene (BaP) pollutant

To evaluate the systemic transport of BaP to the dermis and epidermis of skin substitutes, tissues either in static or perfused conditions were exposed to 10 μM BaP (B1760, Sigma). BaP was added in the DMEM/F12 emersion medium at Day 3 of the emersion phase. A sample of fresh media containing the 10 μM BaP was taken as a control to measure the initial BaP concentration. After 48 h, the media was changed to fresh media containing 10 μM BaP. Samples were cultured for an additional 48 h before harvest. At the end of the culture period, media of each device were sampled to evaluate the remaining BaP after skin culture. The dermis and the epidermis parts were separated and proteins were precipitated using acetonitrile (ACN) (271 004, Sigma). The supernatant was then extracted and analyzed using liquid chromatography with fluorescence detection HPLC-FLD (Shimadzu Prominence- RF-20A-XS). The analytical system was managed by the software Empower® version 3.0. The analytical guard column and analytical column were Pinnacle II PAH (10 × 4,0 mm) and Pinnacle II PAH (150 × 3,2 mm; 4 μm) (Restek, France), respectively. Analyses were carried out with an isocratic elution with mobile phases of ACN/Water 95/5 (v/v). The volume of the injection was variable from 5 to 30 μl and the flow rate was fixed at 1.2 ml min^{-1}. Excitation λ (275 nm) and Emission λ (450 nm) were used for fluorescence detection of BaP.

3. Results

3.1. Development of a full-thickness skin equivalent with three vascular channels and angiogenic sprouts

This study was aimed at creating a full-thickness skin equivalent model with a complex perfusable vascular network as well as a mature epidermal layer. To do so, we used a culture device that allows the reconstruction of a skin equivalent model [28].

First, three nylon wires were strung across connectors to form molds inside this dermis-like layer composed of a mix of human fibroblasts and collagen hydrogel. Once the hydrogel contracted, nylon wires were removed, thereby providing tubular structures used for further perfusion. Knowing that collagen contraction depends on cell number and collagen concentration [61], we adapted fibroblasts concentration to 7.1 × 10^4 ml^{-1} in order to overcome lattice contraction and maintain three opened vascular channels. When normal human keratinocytes (NHK) were seeded on the perfused dermis, the culture medium was optimized to improve epidermal differentiation. In these conditions, histological analyses using HES staining demonstrated that reproducible full-thickness skins were obtained representing a differentiated epidermis and three open microvessels (figure 2). The epidermis displayed all the layers of the differentiation process: (a) organization of cubic cells (proliferative basal keratinocytes) at the basal layer, (b) flattening of these cells in the spinous layer, and (c) development of granular keratinocytes in the granular layer followed by the formation of the stratum corneum (the outermost layer of the epidermis) (figure 2(a)). These histological observations were confirmed by immunostaining the following epidermal markers: keratin 14 (K14), keratin 10 (K10), involucrin (INV), and filaggrin (FLG) were localized at the basal layer, intermediate layers, and upper layers respectively confirming a proper differentiation of the epidermis (figure S1 (available online at stacks.iop.org/BF/13/035042/mmedia)).

The presence of endothelial cells lining the channels was confirmed by positive CD31 immunostaining (figure 2(b)). Immunostaining of the main components of the vascular basement membrane, collagen IV and perlecan, showed a proper deposition of the vascular basal lamina (figure 2(b)).

Then, we sought to promote angiogenic sprouting from these perfusable channels. The potential of endothelial cells to sprout and organize into a vascular network highly depends on the mechanical properties of the surrounded environment. It was shown that matrix densities from 1.2 to 1.9 mg ml^{-1} improves coordinated migration and proliferation of endothelial cells to form stable sprouts, while

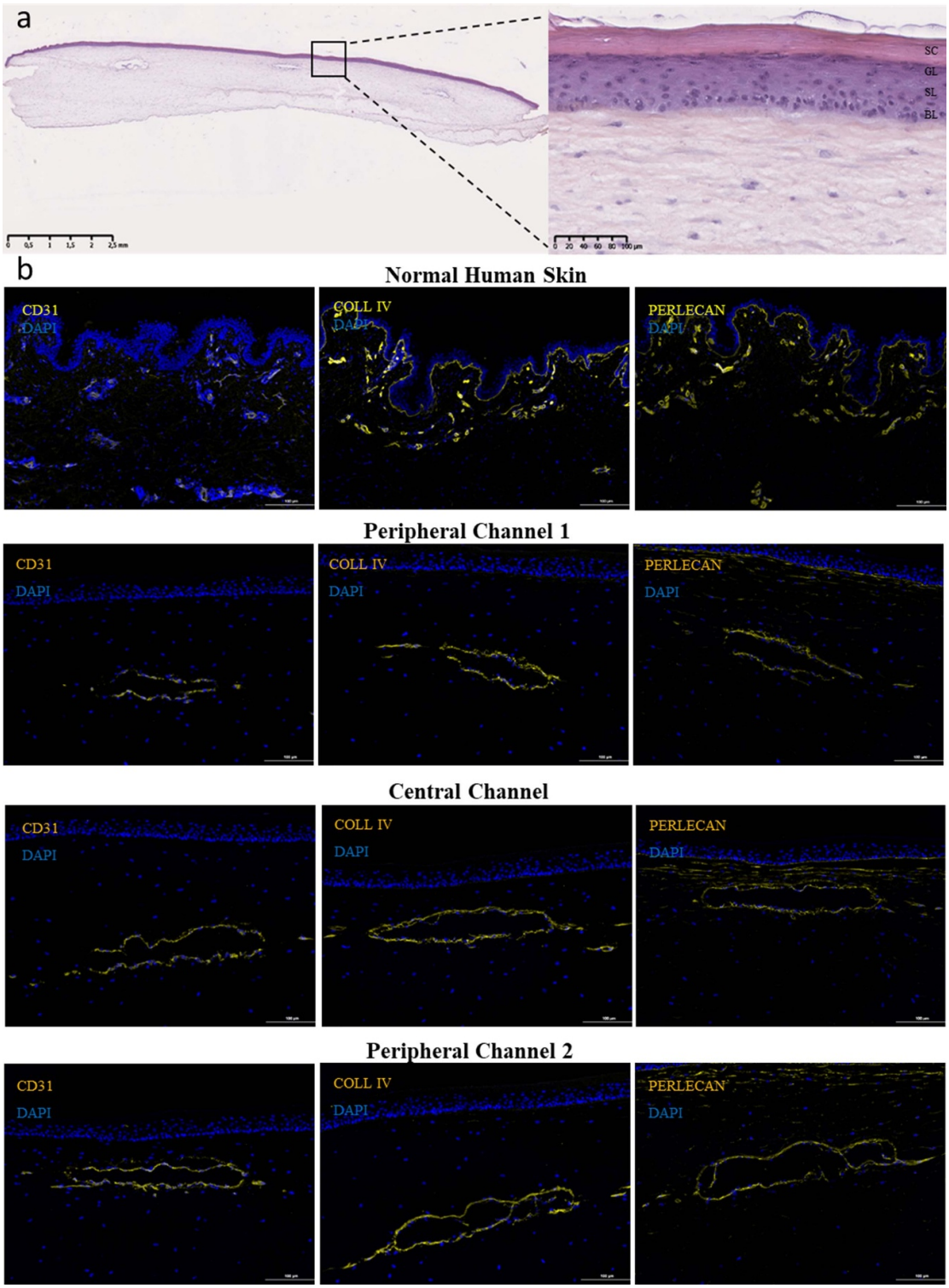

Figure 2. Histological analysis and immunostaining of the skin equivalent with perfusable vascular channels. (a) HES staining of the skin equivalent showing a dermis, an epidermis, and three open microvessels of two skin equivalents. BL = basal layer, SL = spinous layer, GL = granular layer, SC = stratum corneum. (b) Immunostaining of CD31 in endothelial cells and COLL IV and Perlecan as markers of the basal lamina of the three microvessels. Scale bar = 100 μm.

lower densities (0.3–0.7 mg ml^{-1}) or higher densities (2.7 mg ml^{-1}) resulted in uncoordinated migration or cell clusters, respectively [65]. Therefore, collagen concentration (1.5 mg ml^{-1}), as well as the number of endothelial cells seeded in the channels (8.10^5 cells/channel), were optimized in order to promote efficient vascular morphogenesis and sprouting. Using anti-VE-cadherin (VECAD) immunostaining, angiogenic sprouts emanating from vascular channels were characterized (figure 3(a)). These newly formed capillaries could reach up to 800 μm. These sprouts were also marked with collagen IV showing the establishment of a mature basement membrane (figure 3(b)). Sprouts were observed both in

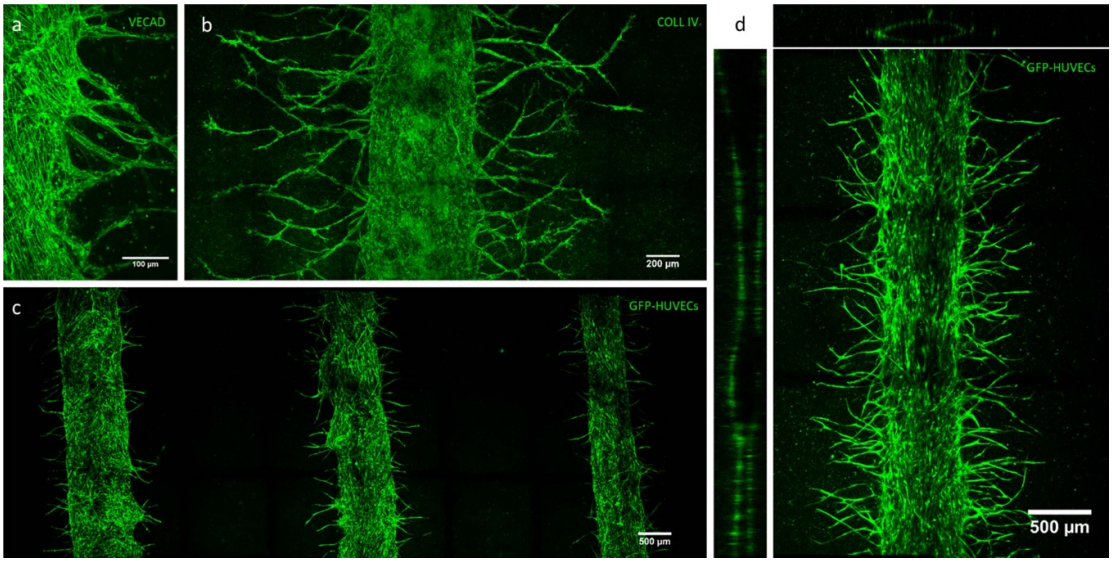

Figure 3. Two-photon microscopy images of angiogenic sprouts from vascular channels. (a) VE-Caderin and (b) COLL IV expression of the main vascular channel and angiogenic sprouts. (c) GFP-HUVECs showing the angiogenic sprouts of the three main vascular channels. (d) Orthogonal sections of the GFP-HUVECs channel showing luminal structures.

peripheral and central channels (figure 3(c)). Orthogonal sections showed opened tubular structure of the main vessel (figure 3(d)).

These results demonstrate that our full-thickness skin model recapitulates a mature epidermis and perfusable vascular channels.

3.2. Generation of a secondary capillary network by vasculogenesis

Our next goal was to further increase the complexity of the vascular network in the skin equivalent. Taking advantage of the auto-assembly properties of endothelial cells seeded into 3D collagen matrices, HUVECS were then seeded between two layers of fibroblasts embedded in a collagen matrix at the same level as the perfused vascular channels. To identify the capillaries formed by angiogenic sprouting from the fluidic channels from those developed by vasculogenesis in the lattice, we used GFP-HUVECs to reconstruct the vascular channels and RFP-HUVECs for the microvascular network between the channels. A mixed media of 1:1 NHDF 3D:ECGM2 was used for the first 5 d of contraction of the vascularized dermis while maintaining the same concentration of growth factors present in both media (figure 1). Using these conditions, a complex RFP-HUVECs microvascular network was formed between the three GFP-HUVECs perfusable vascular channels (figure 4(a)). This dense capillary network displayed connected branches (figure 4(a)) that could also reach and connect to the angiogenic sprouts emanating from the fluidic channels (figure 4(b); Supp Video). The formation of a lumen could be identified by hollow spaces between vascular borders (figure 4(c); Supp Video). The two layers of collagen and fibroblasts were connected with a visible line of cells expressing CD31, perlecan and collagen IV at the location of the microvascular bed (figure 5(a)). The three channels were preserved opened and properly expressed CD31, collagen IV, and perlecan (figure 5(a)). The dermo-epidermal junction (DEJ) was also marked with collagen IV, perlecan, and laminin proving the deposition of basement membrane proteins (figure 5(b)). Moreover, epidermal differentiation was well-maintained and each layer was expressing its specific markers: K14 for the basal layer, K10 for the spinous layer, INV, TGM1, and FIL for the granular layer and stratum corneum (figure 5(c)).

Hence, by combining optimal culture conditions, molding technique using nylon wires, and vasculogenesis, we here developed a full-thickness skin equivalent representing a complex perfusable vascular network with a properly differentiated epidermis.

3.3. Evaluation of skin permeability

Reconstructed skin models can be used for safety and efficacy evaluation of chemicals systematically or topically applied to skin tissues. For topical treatments and bioavailability evaluation, skin barrier function is critical for the percutaneous absorption. However, skin equivalents were proven to have lower epidermal barrier function therefore higher permeability compared to normal human skin [66]. Additionally, these models lack vascular networks and do not allow capillary clearance which plays an important role during ADME process [67, 68].

Here, we evaluated the effect of vascularization and perfusion on epidermal barrier function by studying skin permeation of Caffeine and Minoxidil, two chemicals with different structures and penetration potentials. Four different skin models were

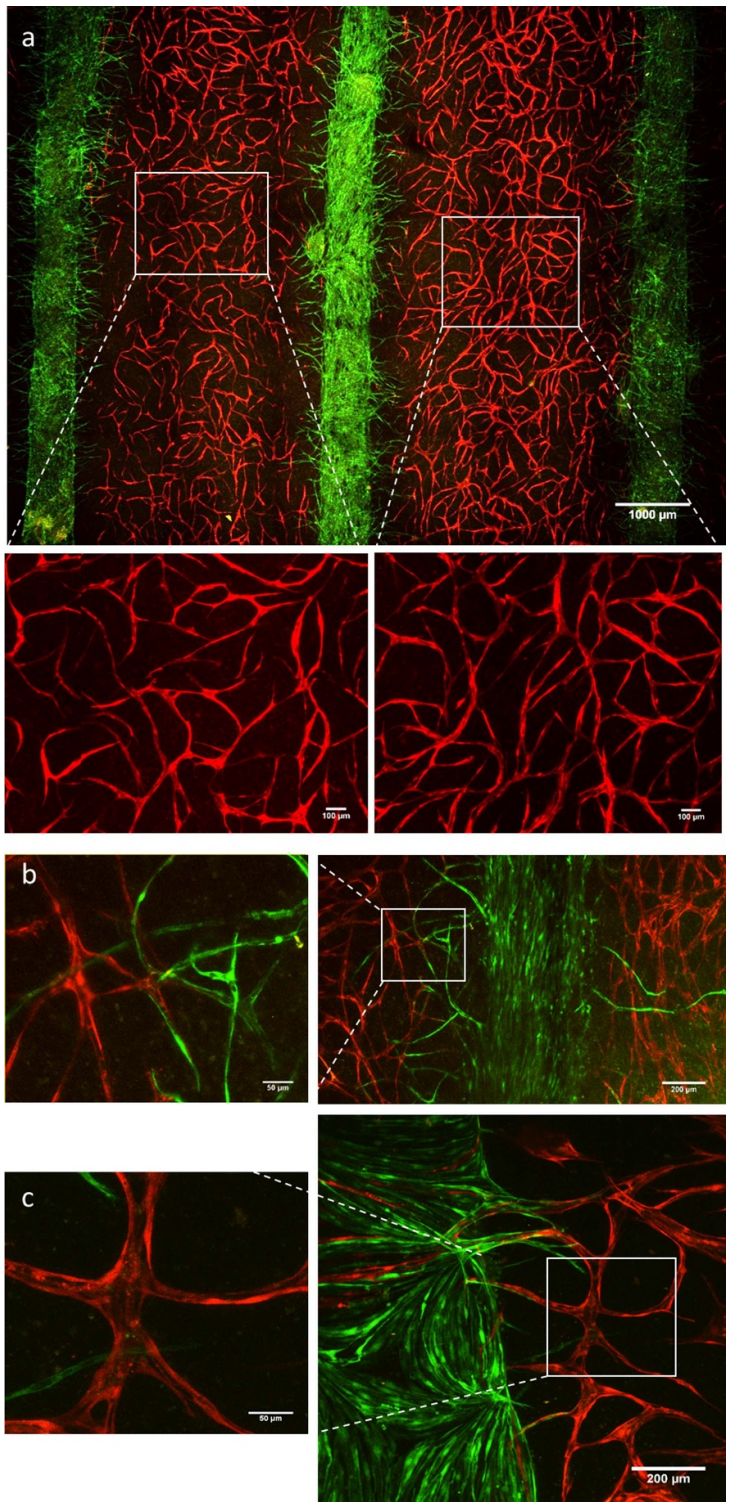

Figure 4. Vasculogenesis of a secondary vascular plexus. (a) Two-photon fluorescence microscopy showing RFP-HUVECs microvascular bed was formed between three GFP-HUVECs perfusable vascular channels. (b) Anastomosis of RFP-HUVECs capillary network and GFP-HUVECs angiogenic sprouts from main channels. (c) High magnification shows hollow space between the borders of the capillaries.

evaluated: control samples with no channels (Lat), channels with endothelial cells without perfusion (ECnoP), perfused channels with endothelial cells (ECP), and perfused channels without endothelial cells (noECP). These models were also compared to porcine ear skin (PES) traditionally used as a surrogate for human skin in the assessment of topical drug bioavailability [69]. Thus, a model with a closer Kp to PES would be a more appropriate alternative for the assessment of skin permeation and penetration *in vitro*.

Results showed that for either Caffeine or Minoxidil, Kp is lower in perfused samples (noECP and ECP) compared to non-perfused samples (ECnoP

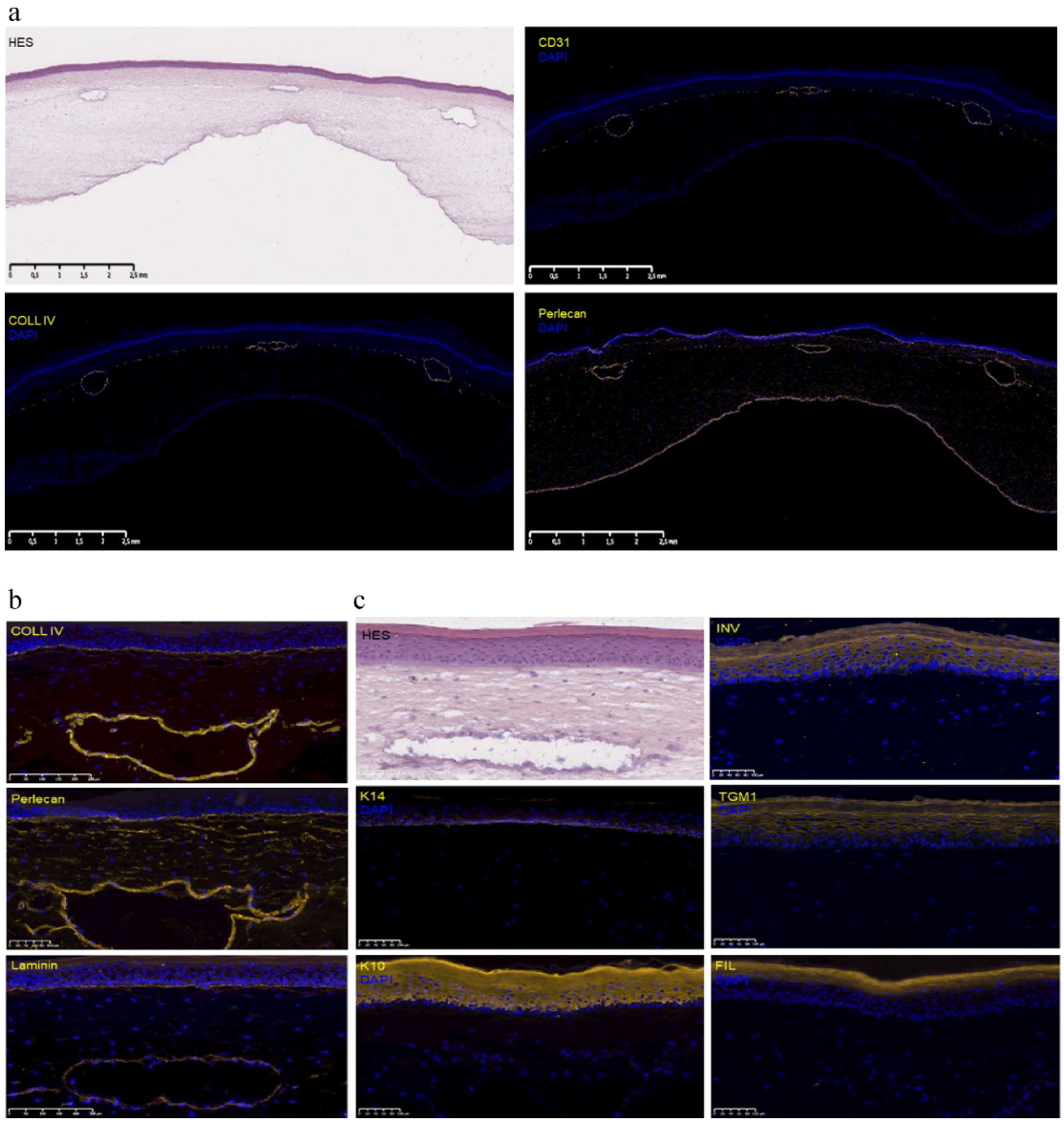

Figure 5. Histological analysis and immunostaining of the skin equivalent with perfusable vascular channels and a secondary vascular plexus. (a) HES staining of the skin equivalent with three perfusable vessels and microvascular bed. Immunostaining of CD31 marker of the endothelial cells, COLL IV, and Perlecan markers of the basal lamina. (b) Immunostaining of COLL IV, Perlecan, and Laminin markers of the vascular basal lamina and the DEJ. (c) HES staining showing epidermal differentiation layers. Immunostaining of K14 marker of the basal layer, K10 marker of the intermediate differentiation, Involucrin, Filaggrin, and TGM1 markers of the late differentiation.

and to Lat). This decrease is significant between perfused samples and ECnoP ($P < 0.05$) whereas it is a tendency with a moderate effect-size between Lat and perfused samples (noECP and ECP) ($P < 0.1$) (figure 6). Interestingly, in static conditions, the presence of vascularized channels (ECnoP) significantly increased Kp for Minoxidil ($P < 0.05$) and tended to increase Kp with a moderate effect size for Caffeine compared to Lat model) ($P < 0.1$) (figure 6). While Kp obtained with the PES remained statistically lower than all skin equivalents, these results showed that perfused reconstructed skin has a lower Kp than non-perfused samples.

We then evaluated the effect of the vascular plexus on epidermal permeability in static (SandnoP) and flow conditions (SandP) (figure 7). As the results between Lat, ECnoP, NoECP, and ECP were similar to previous ones, we only compare them to SandnoP and SandP in this experiment. In the static condition, even if the differences were not significant, the presence of a plexus (SandnoP) tended to increase the Kp of Caffeine and Minoxidil with a moderate or strong effect-size compared to Lat and ECnoP. Similar to previous results, samples' perfusion significantly decreased Kp either for Caffeine or Minoxidil in SandP compared to SandnoP ($P < 0.05$). However, no differences were observed between noECP, ECP, and SandP (figure 7).

Therefore, for both chemicals, we showed that the perfusion of skin equivalents improved the epidermal

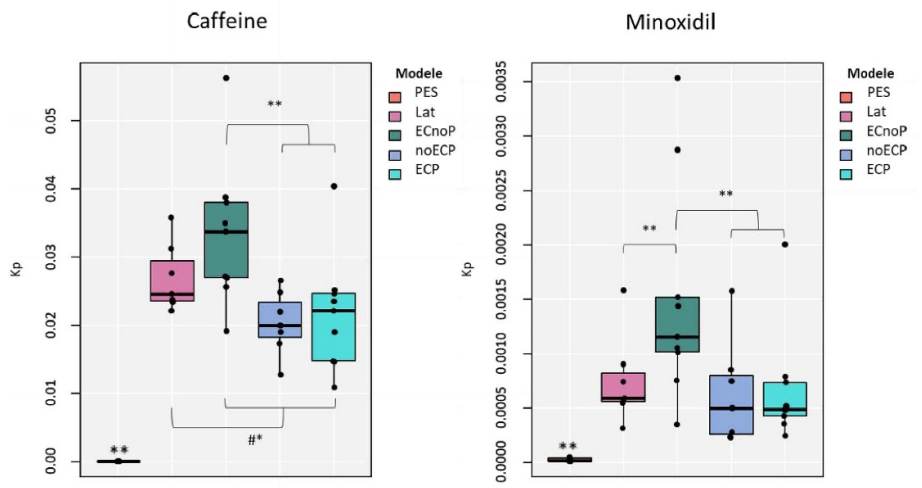

Figure 6. Evaluation of skin permeability. Permeability coefficient Kp (cm h^{-1}) of each of the two chemicals and each skin model. Lat = Control samples with no channels ($N = 7$), ECnoP = Channels with endothelial cells but without perfusion ($N = 9$), ECP = Perfused channels with endothelial cells ($N = 9$), noECP = Perfused channels without endothelial cells ($N = 7$), PES = Porcine ear skin ($N = 8$). $^{*}P < 0.1$, $^{**}P < 0.05$, #moderate effect size.

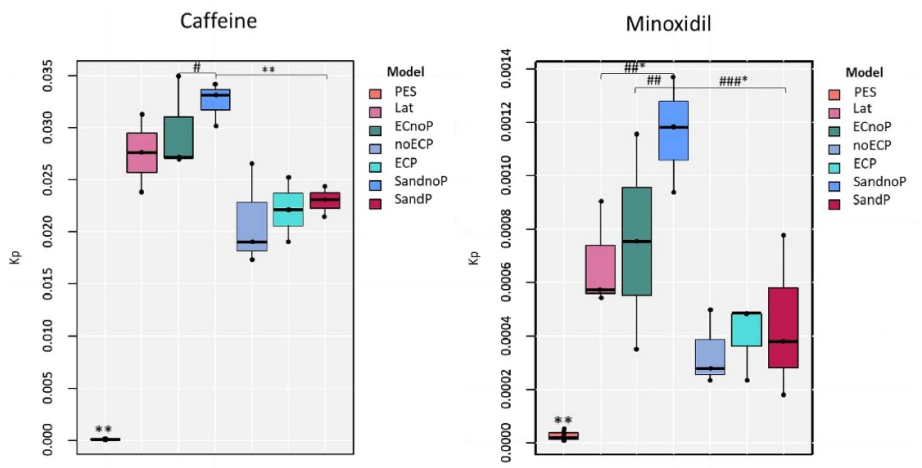

Figure 7. Evaluation of skin permeability. Coefficient of penetration Kp (cm h^{-1}) of each of the two chemicals and each skin model. Lat = Control samples with no channels, ECnoP = Channels with endothelial cells but without perfusion, ECP = Perfused channels with endothelial cells, noECP = Perfused channels without endothelial cells, SandnoP = Channels with endothelial cells and secondary microvascularization without perfusion, SandP = Perfused channels without endothelial cells and secondary microvascularization. PES = Porcine ear skin $^{*}P < 0.1$, $^{**}P < 0.05$, #moderate effect size, ##strong effect size, ###very strong effect size. $N = 3$ for each condition.

barrier or overall skin permeability independently of the presence of ECs and the complexity of the vascular network.

3.4. Evaluation of systemic exposure of a pollutant

Besides topical applications, having a perfusable vascularized skin model holds many interests for systemic exposure either for inflammation studies [70] or drug screening and toxicity assessment [58, 71]. We, therefore, explored the advantage of having, for the first time, perfusable vascular channels, but also a complex microvascular networked in a full-thickness skin equivalent, to estimate dermal and epidermal transport of systemic compounds, specifically, polycyclic aromatic hydrocarbons (PAH) pollutants.

To do so, 10 μM of BaP, a well-known PAH and an extremely widespread environmental and industrial pollutant [72], was added to the culture media of each skin model. After 5 d of exposure, we measured BaP concentration in epidermis, dermis, and culture media. In order to observe the impact of a vascular plexus on BaP distribution, five different models were evaluated: Control samples with no channels (Lat), non-perfused channels with endothelial cells (ECnoP) or with endothelial cells and the secondary vascular plexus (SandnoP), perfused channels with endothelial cells (ECP) or with endothelial cells and the secondary vascular plexus (SandP) (figure 8).

Either in static (figure 8(a)) or fluidic conditions (figure 8(b)), the presence of a secondary vascular

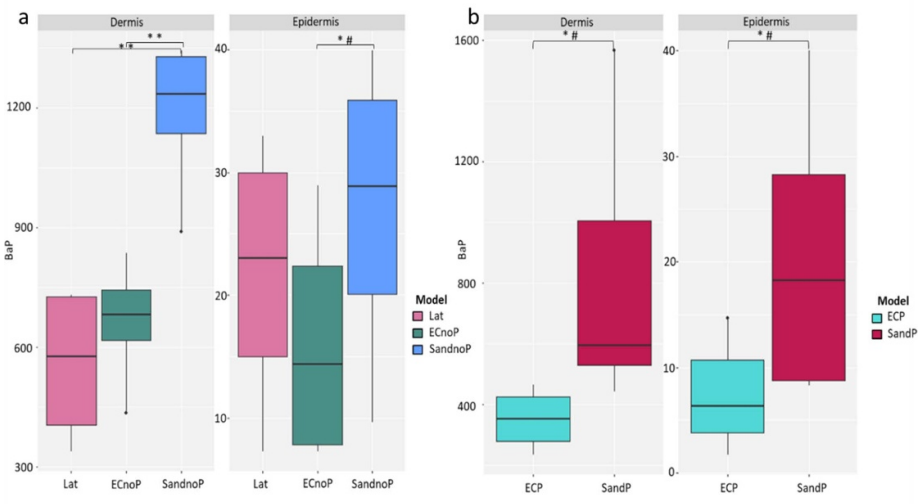

Figure 8. Evaluation of systemic delivery of pollutants. Graphical box plot presentation of BaP concentrations (ng ml^{-1}) in the dermis or epidermis either in static models (a) or perfused models (b). Lat = Control samples with no channels, ECnoP = Channels with endothelial cells but without perfusion, ECP = Perfused channels with endothelial cells, SandnoP = Channels with endothelial cells and secondary microvascularization without perfusion, SandP = Perfused channels without endothelial cells and secondary microvascularization. $^{*}P < 0.1$, $^{**}P < 0.05$, #moderate effect size. $N = 6$ for each condition.

plexus (SandnoP and SandP) increased BaP delivery either in the dermis or the epidermis compared to samples without channels (Lat) or with the three vascular channels only (ECnoP and ECP). This increase of distribution is significant in the static dermal layer and is a tendency with moderate effect-size in the epidermal layer (static or perfused conditions) and the perfused dermal layer. However, with (SandP) or without (ECP) a secondary vascular plexus, BaP concentrations found in perfused samples were lower than in static conditions (figure 8(b)). These results are consistent with the concentrations found in the culture media (figure S2(a)). Previous internal studies showed that being highly hydrophobic, BaP is extremely adherent to plastic (data not shown). Therefore, the low concentrations found in perfused samples could be due to BaP absorption by silicon tubes used for peristaltic perfusion. To measure the loss of BaP in the tubing, a control experiment was set with all the setups of the classic culture (devices, culture dishes, silicon tubes, and media) but without the skin. We found that in fluidic culture either with 2.4 or 6.5 ml h^{-1}, BaP was ten times lower than static culture (figure S2(b)).

Thus, in this experiment, fluidic and static conditions could not be compared as the skin is exposed to different concentrations of BaP during the culture. However, these results proved that the presence of a complex vascular plexus increases systemic diffusion of the pollutant either in the dermis or the epidermis.

4. Discussion

Currently, 2D and 3D *in vitro* skin models are used to replace animal testing both in pharmaceutical and cosmetic companies. Commercialized skin models which resulted in major advances in the field of skin engineering are available (e.g. EpiSkin®, SkinEthic® and T-Skin® (L'Oreal, France), Epi-Derm® (MatTek Corporation, USA), epiCS® (CellSystems, Germany), Phenion® (Henkel, Germany), NeoDerm® (Tegoscience, Korea), LabCyte® (J-TEC, Japan)). These models have the advantage of being highly stable and reproducible as they represent mono or bi-layered constructs with simple cell composition. However, the lack of complexity of the *in vivo* skin as appendages, vasculature, cells' variety, and distribution, is a limitation for the predictivity and relevance of *in vitro* applications. In this report, we developed a vascularized full-thickness skin model that comprises for the first time a differentiated epidermis, perfusable vessels, and a secondary microvascular network.

As reconstructed skin models are specifically used for safety and efficacy evaluation of chemicals, applied systematically or topically to skin tissues, the functionality of the vascularized skin equivalent for *in vitro* assessments was evaluated with topical and systemic applications.

One important readout for topical application is the estimation of new compounds' skin absorption including skin distribution, metabolism, and elimination from the skin into systemic circulation. However, existing skin models have a higher permeation than *in vivo* skin [73] which could be related to a barrier function default. We, therefore, evaluated the effect of vascularization and perfusion on epidermal barrier integrity by evaluating the percutaneous absorption of caffeine (high permeability chemical compound) and minoxidil (low permeability chemical compound). For both chemicals, we

showed that percutaneous absorption is lower in perfused samples. This could be due to an improvement of epidermal barrier function or the overall skin permeability. In any case, these results suggest that perfused skin models are a better alternative for the assessment of skin permeability and penetration *in vitro* compared to non-perfused models. This is consistent with other studies showing the beneficial effect of fluidic cultures on the epidermal barrier function [18, 74]. Indeed, besides improving nutrients and oxygen supply, media perfusion was shown to enhance the deposition of DEJ proteins [18] which is crucial for the basement membrane integrity and epidermal differentiation. It was also proven to increase cell viability and tight junction formation [74] as well as the expression of epidermal markers and stratum corneum thickness [75]. Additionally, the shear stress induced by dynamic culture can also affect epidermal maturation and barrier function [14, 18, 75]. However, in our experiments presence of ECs in non-perfused conditions seemed to lower the efficacy of the barrier function. We hypothesized that the presence of endothelial cells may delay the maturation of the epidermis as both cell types share common growth factors like EGF, insulin or hydrocortisone. In fact, in static conditions, media diffuses through the dermis. Therefore, growth factors could gradually be depleted by endothelial cells. This could also explain why additional ECs in the secondary vascular plexus further increased the penetration of chemicals. To confirm this hypothesis, samples with ECs could be cultured for a longer period to measure whether we find the same permeability as non-vascularized samples.

In this study, we measured the concentration of chemicals in static media beneath the skin. However, we could also evaluate percutaneous penetration and systemic concentration of compounds in the vascular channel underflow which could better mimic capillary clearance and improve safety evaluation. In fact, after topical application, some chemicals are absorbed and/or metabolized and reach the systemic circulation. Under certain concentrations, these chemicals could cause side effects on other distant organs [76]. Therefore, a skin model with a closer permeation to *in vivo* physiology would allow a better prediction of systemic toxicity.

Besides topical applications, having a perfusable vascularized skin model holds many interests for systemic applications. Most of the existing skin models are cultured in static conditions which is not representative of the *in vivo* reality [58]. Additionally, substances are usually added to static culture media in contact with all the surface of dermis equivalents whereas, *in vivo*, systemic substances are delivered via the vascular network meaning that they are exposed to blood flow and have the vessel wall as an additional diffusion barrier. In that sense, skin-on-a-chip platforms were used to mimic blood flow for topical and systemic studies [14, 18, 20]. However, in these platforms, fluidic media passes beneath the skin-equivalent whilst *in vivo,* it circulates through the dermis in confined tube-shaped microvessels. Most of the time, culture media is also separated from the skin by a permeable membrane that could introduce a supplemental and non-physiological barrier for substance diffusion. On the other hand, the few existing skin models representing perfusable vessels for systemic delivery of drugs were limited to macro-channels located in the dermis [28, 58, 60]. Lack of micro-vascularization could result in misleading and/or irrelevant drug delivery estimation compared to the *in vivo* situation. To show the advantage of having a complex vasculature, we exposed our vascularized skin model to BaP in order to mimic systemic exposure to pollutants. Pollutants like BaP can promote photoreactivity and phototoxicity with nanomolar range concentrations [72]. Various studies have shown that a combined exposure of pollutants and UVs could be toxic and aggravate sunlight-induced skin damage [72, 77–79]. However, these studies were investigated either *in vivo*, in 2D cell culture, or 3D epidermal equivalents whereas UVs and especially UVA (UVA1 and UVA2) wavelength are capable to reach the dermal layer [80]. Moreover, BaP was measured in the blood of smokers and individuals living in polluted areas [81, 82]. This suggests that the skin could be exposed to these pollutants from the surface but also the systemic circulation. Therefore, having a complex vascular structure in a dermal equivalent allows a better understanding of BaP transport and its effects on the dermis before reaching the epidermal layer. Indeed, we found that either in static or fluidic conditions, the presence of the secondary vascular plexus increased the presence of benzo[a]pyren BaP in the dermis and the epidermis compared to samples without vessels or with the three vascular channels alone. This suggests that having a finer vascular structure makes the systemic delivery of substances to or from the skin more efficient. This could apply not only to pollutants but to any drugs and compounds systemically delivered.

We, therefore, demonstrated that our vascularized full-thickness skin is a valuable model for topical or systemic assessments. In this study, we focused on the systemic delivery and transdermal absorption of compounds. However, a broad range of applications is possible either for knowledge studies or efficacy and safety evaluations. For instance, vascularized skin models could also serve to study wound healing, skin regeneration as well as the molecular mechanisms involved. In fact, 3D skin reconstructs were already used to mimic the wound healing process in *in vitro* trauma models [83]. However, these models do not represent the local microenvironment

of *in vivo* wounds and cannot predict the side effect of the therapeutic treatment due to the lack of vascularization, systemic circulation, and inflammation mediators, widely reported as critical components during the wound healing process [84]. Therefore, including a vascular network and systemic perfusion to reconstructed skin models could improve the efficiency of screening therapeutic compounds and the prediction rate of patient's responses to such treatments. Besides screening therapeutic compounds for wound healing, having both angiogenesis and vasculogenesis processes in the same skin model could improve the screening of pro and antiangiogenic drugs. Indeed, vascularization plays an important role in tumor growth and metastasis [85]. Therefore, this model could be used to better understand tumor, stroma, and endothelial cells' interactions in non-melanoma skin cancer. In addition, this complex vascularized skin model could also be beneficial for the integration of skin appendages that require blood supply. For instance, without prevascularization and perfusion, generating an *in vitro* skin-equivalent with hair follicles density equivalent to the *in vivo* situation could result in necrosis [10]. Indeed, fluidic systems have proven to prolong the culture period of *ex vivo* hair follicles and postpone the initiation of the hair follicle regression phase (catagen) compared to static conditions [14].

Our skin model represents an advanced step compared to existing models but it also includes limitations. Indeed, numerous parameters might further be improved. HUVECs were used as they are quite easy to access and their culture condition is well-known. Nevertheless, HUVECs could be replaced by human dermal microvascular endothelial cells which would be more relevant for a skin model. In fact, HUVECs are isolated from large vessels whereas dermis vasculature mainly consists of microvessels [31]. Vessel diameter is not the only difference, but this parameter could influence cell behavior as it was already shown that endothelial cells from different blood vessels or different tissues have distinct gene expression profiles [86]. Bioprinting could also be used as a replacement of the molding technique to create functional a vascular network that would contain a more complex architecture (smaller vessel diameters and improved spatial control of their distribution) compared to tubular channels [87]. Moreover, arteries, veins, and lymphatic vessels could be created using multi-channels. Indeed, engineering reconstructed tissues with both blood and lymphatic capillaries was previously reported [88–90]. Finally, besides optimization of skin reconstruction, the device could also be improved to be able to separate the culture media surrounding the skin equivalent from the one perfusing the vascular channels. This improvement would better mimic skin physiology and open the possibilities for new applications requiring immune cells perfusion.

5. Conclusion

We developed for the first time a full-thickness human skin model with a mature epidermis and three tubular structures with angiogenic sprouts that can be perfused, associated with a complex microvascular network. The integrity of each compartment was confirmed by histological immunofluorescence analysis and compared to normal human skin. We proved that having a perfusable vasculature closer to the *in vivo* vascular plexus resulted in a more reliable model for topical and systemic assessments. This includes a wide range of applications either for knowledge or efficacy and safety studies.

Data availability statement

The data that support the findings of this study are available upon reasonable request from the authors.

Acknowledgments

We greatly appreciate Nobuhito Mori for his advice and technical support. We thank Florence Berthelot for her help in HUVECS transduction, Samia Boudah for her support in HPLC-Fluo analysis and France Maloumian for her support in schematizing the protocol. We are grateful to Sébastien Grégoire for fruitful discussions and analysis of skin permeability assays. We also thank Julien Demaude and Alexandre Nicolas for their contribution in the initiation of this project.

ORCID iDs

Sacha Salameh https://orcid.org/0000-0002-3162-994X
Shoji Takeuchi https://orcid.org/0000-0001-6946-0409

References

[1] Meyer U 2009 The History of Tissue Engineering and Regenerative Medicine in Perspective Fundamentals of Tissue Engineering and Regenerative Medicine (Berlin: Springer) pp 5–12
[2] Albanna M and Holmes J H IV 2016 *Skin Tissue Engineering and Regenerative Medicine* (Boston: Academic Press) pp 1–443
[3] Groeber F, Holeiter M, Hampel M, Hinderer S and Schenke-Layland K 2011 Skin tissue engineering—*in vivo* and *in vitro* applications *Adv. Drug. Deliv. Rev.* **63** 352–66
[4] Yousuf Y *et al* 2018 2—Overall perspective on the clinical importance of skin models *Skin Tissue Models* ed A P Marques (New York: Academic) pp 39–54
[5] Pellevoisin C *et al* 2018 1—Cosmetic industry requirements regarding skin models for cosmetic testing *Skin Tissue Models* ed A P Marques (New York: Academic) pp 3–37
[6] Rheinwald J G and Green H 1975 Serial cultivation of strains of human epidermal keratinocytes: the formation of keratinizing colonies from single cells *Cell* **6** 331–43
[7] Black A F, Berthod F, L'Heureux N, Germain L and Auger F A 1998 *In vitro* reconstruction of a human

capillary-like network in a tissue-engineered skin equivalent *Faseb. J.* **12** 1331–40
[8] Regnier M, Staquet M-J, Schmitt D and Schimdt R 1997 Integration of Langerhans cells into a pigmented reconstructed human epidermis *J. Invest. Dermatol.* **109** 510–2
[9] Bertaux B, Morliere P, Moreno G, Courtalon A, Masse J M and Dubertret L 1988 Growth of melanocytes in a skin equivalent model *in vitro Br. J. Dermatol.* **119** 503–12
[10] Abaci H E, Coffman A, Doucet Y, Chen J, Jacków J, Wang E, Guo Z, Shin J U, Jahoda C A and Christiano A M 2018 Tissue engineering of human hair follicles using a biomimetic developmental approach *Nat. Commun.* **9** 5301
[11] Huber B, Link A, Linke K, Gehrke S A, Winnefeld M and Kluger P J 2016 Integration of mature adipocytes to build-up a functional three-layered full-skin equivalent *Tissue Eng.* C **22** 756–64
[12] Albouy M, Tanguy M, Onteniente B, Thepot A, Maruotti J and Dos Santos M 2018 Development of A 3D full-thickness skin equivalent model containing sebocyte organoids derived from human ips cells *J. Invest. Dermatol.* **138** B24
[13] Muller Q, Beaudet M-J, De Serres-Bérard T, Bellenfant S, Flacher V and Berthod F 2018 Development of an innervated tissue-engineered skin with human sensory neurons and schwann cells differentiated from iPS cells *Acta Biomater.* **82** 93–101
[14] Atac B, Wagner I, Horland R, Lauster R, Marx U, Tonevitsky A G, Azar R P and Lindner G 2013 Skin and hair on-a-chip: *in vitro* skin models versus ex vivo tissue maintenance with dynamic perfusion *Lab Chip* **13** 3555–61
[15] Wagner I *et al* 2013 A dynamic multi-organ-chip for long-term cultivation and substance testing proven by 3D human liver and skin tissue co-culture *Lab Chip* **13** 3538–47
[16] Lee S, Jin S-P, Kim Y K, Sung G Y, Chung J H and Sung J H 2017 Construction of 3D multicellular microfluidic chip for an *in vitro* skin model *Biomed. Microdevices* **19** 22
[17] Jeong Song H *et al* 2017 Development of 3D skin-equivalent in a pump-less microfluidic chip *J. Ind. Eng. Chem.* **60** 355–59
[18] Sriram G, Alberti M, Dancik Y, Wu B, Wu R, Feng Z, Ramasamy S, Bigliardi P L, Bigliardi-Qi M and Wang Z 2018 Full-thickness human skin-on-chip with enhanced epidermal morphogenesis and barrier function *Mater. Today* **21** 326–40
[19] Sung J H, Esch M B, Prot J-M, Long C J, Smith A, Hickman J J and Shuler M L 2013 Microfabricated mammalian organ systems and their integration into models of whole animals and humans *Lab Chip* **13** 1201–12
[20] Abaci H E, Gledhill K, Guo Z, Christiano A M and Shuler M L 2015 Pumpless microfluidic platform for drug testing on human skin equivalents *Lab Chip* **15** 882–8
[21] Abaci H E, Guo Z, Doucet Y, Jacków J and Christiano A 2017 Next generation human skin constructs as advanced tools for drug development *Exp. Biol. Med.* **242** 1657–68
[22] Lovett M, Lee K, Edwards A and Kaplan D L 2009 Vascularization strategies for tissue engineering *Tissue Eng. B* **15** 353–70
[23] Min S, Ko I K and Yoo J J 2019 State-of-the-art strategies for the vascularization of three-dimensional engineered organs *Vasc. Spec. Int.* **35** 77–89
[24] Rouwkema J and Khademhosseini A 2016 Vascularization and angiogenesis in tissue engineering: beyond creating static networks *Trends Biotechnol.* **34** 733–45
[25] Liu J, Zheng H, Poh P, Machens H-G and Schilling A 2015 Hydrogels for engineering of perfusable vascular networks *Int. J. Mol. Sci.* **16** 15997–6016
[26] Auger F A, Gibot L and Lacroix D 2013 The pivotal role of vascularization in tissue engineering *Annu. Rev. Biomed. Eng.* **15** 177–200
[27] Amann A *et al* 2017 Development of a 3D angiogenesis model to study tumour—endothelial cell interactions and the effects of anti-angiogenic drugs *Sci. Rep.* **7** 2963
[28] Mori N, Morimoto Y and Takeuchi S 2017 Skin integrated with perfusable vascular channels on a chip *Biomaterials* **116** 48–56
[29] Massa S *et al* 2017 Bioprinted 3D vascularized tissue model for drug toxicity analysis *Biomicrofluidics* **11** 044109
[30] Dai N-T *et al* 2018 Development of a novel pre-vascularized three-dimensional skin substitute using blood plasma gel *Cell Transplant.* **27** 1535–47
[31] Bourland J *et al* 2018 8—Strategies to promote the vascularization of skin substitutes after transplantation *Skin Tissue Models* ed A P Marques (New York: Academic) pp 177–200
[32] Li W, Lan Y, Guo R, Zhang Y, Xue W and Zhang Y 2015 *in vitro* and *in vivo* evaluation of a novel collagen/cellulose nanocrystals scaffold for achieving the sustained release of basic fibroblast growth factor *J. Biomater. Appl.* **29** 882–93
[33] Joshi V S, Lei N Y, Walthers C M, Wu B and Dunn J C Y 2013 Macroporosity enhances vascularization of electrospun scaffolds *J. Surg. Res.* **183** 18–26
[34] Griffin M, Palgrave R, Baldovino-Medrano V, Butler P and Kalaskar D 2018 Argon plasma improves the tissue integration and angiogenesis of subcutaneous implants by modifying surface chemistry and topography *Int. J. Nanomed.* **13** 6123–41
[35] Cam C, Zhu S, Truong N F, Scumpia P O and Segura T 2015 Systematic evaluation of natural scaffolds in cutaneous wound healing *J. Mater. Chem.* B **3** 7986–92
[36] Suh W *et al* 2005 Transplantation of endothelial progenitor cells accelerates dermal wound healing with increased recruitment of monocytes/macrophages and neovascularization *Stem Cells* **23** 1571–8
[37] Sieveking D P, Buckle A, Celermajer D S and Ng M K C 2008 Strikingly different angiogenic properties of endothelial progenitor cell subpopulations: insights from a novel human angiogenesis assay *J. Am. Coll. Cardiol.* **51** 660–8
[38] Cao Y, Sun Z, Liao L, Meng Y, Han Q and Zhao R C 2005 Human adipose tissue-derived stem cells differentiate into endothelial cells *in vitro* and improve postnatal neovascularization *in vivo Biochem. Biophys. Res. Commun.* **332** 370–9
[39] Jean J 2013 Bioengineered skin: the self-assembly approach *J. Tissue Sci. Eng.* **03** S5:001
[40] Hikimoto D, Nishiguchi A, Matsusaki M and Akashi M 2016 High-throughput blood- and lymph-capillaries with open-ended pores which allow the transport of drugs and cells *Adv. Healthcare Mater.* **5** 1969–78
[41] Miyazaki H, Tsunoi Y, Akagi T, Sato S, Akashi M and Saitoh D 2019 A novel strategy to engineer pre-vascularized 3-dimensional skin substitutes to achieve efficient, functional engraftment *Sci. Rep.* **9** 7797
[42] Schultheiss D *et al* 2005 Biological vascularized matrix for bladder tissue engineering: matrix preparation, reseeding technique and short-term implantation in a porcine model *J. Urol.* **173** 276–80
[43] Groeber F *et al* 2016 A first vascularized skin equivalent as an alternative to animal experimentation *ALTEX* **33** 415–22
[44] Gershlak J R *et al* 2017 Crossing kingdoms: using decellularized plants as perfusable tissue engineering scaffolds *Biomaterials* **125** 13–22
[45] Uygun B E *et al* 2010 Organ reengineering through development of a transplantable recellularized liver graft using decellularized liver matrix *Nat. Med.* **16** 814–20
[46] Skardal A, Zhang J and Prestwich G D 2010 Bioprinting vessel-like constructs using hyaluronan hydrogels crosslinked with tetrahedral polyethylene glycol tetracrylates *Biomaterials* **31** 6173–81
[47] Hinton T J *et al* 2015 Three-dimensional printing of complex biological structures by freeform reversible embedding of suspended hydrogels *Science Advances* **1** e1500758
[48] Zhang Y, Yu Y, Akkouch A, Dababneh A, Dolati F and Ozbolat I T 2015 *In vitro* study of directly bioprinted perfusable vasculature conduits *Biomater. Sci.* **3** 134–43

[49] Chrobak K M, Potter D R and Tien J 2006 Formation of perfused, functional microvascular tubes *in vitro Microvasc. Res.* **71** 185–96
[50] Zheng Y *et al* 2012 *In vitro* microvessels for the study of angiogenesis and thrombosis *Proc. Natl Acad. Sci. USA* **109** 9342–7
[51] Du Y, Ghodousi M, Qi H, Haas N, Xiao W and Khademhosseini A 2011 Sequential assembly of cell-laden hydrogel constructs to engineer vascular-like microchannels *Biotechnol. Bioeng.* **108** 1693–703
[52] Tocchio A, Tamplenizza M, Martello F, Gerges I, Rossi E, Argentiere S, Rodighiero S, Zhao W, Milani P and Lenardi C 2015 Versatile fabrication of vascularizable scaffolds for large tissue engineering in bioreactor *Biomaterials* **45** 124–31
[53] Gibot L, Galbraith T, Kloos B, Das S, Lacroix D A, Auger F A and Skobe M 2016 Cell-based approach for 3D reconstruction of lymphatic capillaries *in vitro* reveals distinct functions of HGF and VEGF-C in lymphangiogenesis *Biomaterials* **78** 129–39
[54] Klar A S, Güven S, Biedermann T, Luginbühl J, Böttcher-Haberzeth S, Meuli-Simmen C, Meuli M, Martin I, Scherberich A and Reichmann E 2014 Tissue-engineered dermo-epidermal skin grafts prevascularized with adipose-derived cells *Biomaterials* **35** 5065–78
[55] Kim B S, Kwon Y W, Kong J-S, Park G T, Gao G, Han W, Kim M-B, Lee H, Kim J H and Cho D-W 2018 3D cell printing of *in vitro* stabilized skin model and *in vivo* pre-vascularized skin patch using tissue-specific extracellular matrix bioink: a step towards advanced skin tissue engineering *Biomaterials* **168** 38–53
[56] Skardal A, Zhang J, McCoard L, Xu X, Oottamasathien S and Prestwich G D 2010 Photocrosslinkable hyaluronan-gelatin hydrogels for two-step bioprinting *Tissue Eng.* A **16** 2675–85
[57] Lee V K, Lanzi A M, Ngo H, Yoo -S-S, Vincent P A and Dai G 2014 Generation of multi-scale vascular network system within 3D hydrogel using 3D bio-printing technology *Cell Mol. Bioeng.* **7** 460–72
[58] Abaci H E, Guo Z, Coffman A, Gillette B, Lee W-H, Sia S K and Christiano A M 2016 Human skin constructs with spatially controlled vasculature using primary and iPSC-derived endothelial cells *Adv. Healthcare Mater.* **5** 1800–7
[59] Mori N, Morimoto Y and Takeuchi S 2018 Perfusable and stretchable 3D culture system for skin-equivalent *Biofabrication* **11** 011001
[60] Kim B S, Gao G, Kim J Y and Cho D-W 2019 3D cell printing of perfusable vascularized human skin equivalent composed of epidermis, dermis, and hypodermis for better structural recapitulation of native skin *Adv. Healthcare Mater.* **8** e1801019
[61] Bell E, Ivarsson B and Merrill C 1979 Production of a tissue-like structure by contraction of collagen lattices by human fibroblasts of different proliferative potential *in vitro Proc. Natl Acad. Sci. USA* **76** 1274–8
[62] Asselineau D, Bernhard B, Bailly C and Darmon M 1985 Epidermal morphogenesis and induction of the 67 kD keratin polypeptide by culture of human keratinocytes at the liquid-air interface *Exp. Cell Res.* **159** 536–9
[63] Scientific Committee on Consumer Safety 2010 Basic criteria for the in vitro assessment of dermal absorption of cosmetic ingredients
[64] Korinth G, Schaller K H and Drexler H 2005 Is the permeability coefficient Kp a reliable tool in percutaneous absorption studies? *Arch. Toxicol.* **79** 155–9
[65] Shamloo A and Heilshorn S C 2010 Matrix density mediates polarization and lumen formation of endothelial sprouts in VEGF gradients *Lab Chip* **10** 3061–8
[66] Godin B and Touitou E 2007 Transdermal skin delivery: predictions for humans from *in vivo*, *ex vivo* and animal models *Adv. Drug Delivery Rev.* **59** 1152–61
[67] Kretsos K and Kasting G B 2005 Dermal capillary clearance: physiology and modeling *Skin Pharmacol. Physiol.* **18** 55–74
[68] Kretsos K, Miller M A, Zamora-Estrada G and Kasting G B 2008 Partitioning, diffusivity and clearance of skin permeants in mammalian dermis *Int. J. Pharm.* **346** 64–79
[69] Flaten G E, Palac Z, Engesland A, Filipović-Grčić J, Vanić Ž and Škalko-Basnet N 2015 *In vitro* skin models as a tool in optimization of drug formulation *Eur. J. Pharm. Sci.* **75** 10–24
[70] Wufuer M, Lee G, Hur W, Jeon B, Kim B J, Choi T H and Lee S 2016 Skin-on-a-chip model simulating inflammation, edema and drug-based treatment *Sci. Rep.* **6** 37471
[71] Cochrane A, Albers H J, Passier R, Mummery C L, van den Berg A, Orlova V V and van der Meer A D 2019 Advanced *in vitro* models of vascular biology: human induced pluripotent stem cells and organ-on-chip technology *Adv. Drug. Deliv. Rev.* **140** 68–77
[72] Soeur J *et al* 2017 Photo-pollution stress in skin: traces of pollutants (PAH and particulate matter) impair redox homeostasis in keratinocytes exposed to UVA1 *J. Dermatol. Sci.* **86** 162–9
[73] Schafer-Korting M *et al* 2008 The use of reconstructed human epidermis for skin absorption testing: results of the validation study *Altern. Lab. Anim.* **36** 161–87
[74] Ramadan Q and Ting F C 2016 *In vitro* micro-physiological immune-competent model of the human skin *Lab Chip* **16** 1899–908
[75] Strüver K, Friess W and Hedtrich S 2017 Development of a perfusion platform for dynamic cultivation of *in vitro* skin models *Skin Pharmacol. Physiol.* **30** 180–9
[76] Hewitt P and Maibach H I 2000 *Systemic Toxicity* (Berlin: Springer)
[77] Burke K E and Wei H 2009 Synergistic damage by UVA radiation and pollutants *Toxicol. Ind. Health* **25** 219–24
[78] Botta C, Di Giorgio C, Sabatier A-S and De Méo M 2009 Effects of UVA and visible light on the photogenotoxicity of benzo[a]pyrene and pyrene *Environ. Toxicol.* **24** 492–505
[79] Wang S, Sheng Y, Feng M, Leszczynski J, Wang L, Tachikawa H and Yu H 2007 Light-induced cytotoxicity of 16 polycyclic aromatic hydrocarbons on the US EPA priority pollutant list in human skin HaCaT keratinocytes: relationship between phototoxicity and excited state properties *Environ. Toxicol.* **22** 318–27
[80] Herlin C, Sauniere D and Huertas D 2009 Xeroderma pigmentosum: radical therapeutic procedure on the face using artificial skin *Ann. Chir. Plast. Esthet.* **54** 594–9
[81] Song X F, Chen Z Y, Zang Z J, Zhang Y N, Zeng F, Peng Y P and Yang C 2013 Investigation of polycyclic aromatic hydrocarbon level in blood and semen quality for residents in Pearl River Delta region in China *Environ. Int.* **60** 97–105
[82] Guo Y, Huo X, Wu K, Liu J, Zhang Y and Xu X 2012 Carcinogenic polycyclic aromatic hydrocarbons in umbilical cord blood of human neonates from Guiyu, China *Sci. Total Environ.* **427-428** 35–40
[83] Laplante A F, Germain L, Auger F A and Moulin V 2001 Mechanisms of wound reepithelialization: hints from a tissue-engineered reconstructed skin to long-standing questions *Faseb. J.* **15** 2377–89
[84] Tonnesen M G, Feng X and Clark R A 2000 Angiogenesis in wound healing *J. Invest. Dermatol. Symp. Proc.* **5** 40–46
[85] Bielenberg D R and Zetter B R 2015 The contribution of angiogenesis to the process of metastasis *Cancer J.* **21** 267–73
[86] Chi J-T *et al* 2003 Endothelial cell diversity revealed by global expression profiling *Proc. Natl Acad. Sci.* **100** 10623
[87] Grigoryan B *et al* 2019 Multivascular networks and functional intravascular topologies within biocompatible hydrogels *Science* **364** 458–64
[88] Knezevic L, Schaupper M, Mühleder S, Schimek K, Hasenberg T, Marx U, Priglinger E, Redl H and Holnthoner W 2017 Engineering blood and lymphatic microvascular networks in fibrin matrices *Front. Bioeng. Biotechnol.* **5** 25

[89] Bourland J, Fradette J and Auger F A 2018 Tissue-engineered 3D melanoma model with blood and lymphatic capillaries for drug development *Sci. Rep.* **8** 13191

[90] Marino D, Luginbuhl J, Scola S, Meuli M and Reichmann E 2014 Bioengineering dermo-epidermal skin grafts with blood and lymphatic capillaries *Sci. Transl. Med.* **6** 221ra14